Soft Matter

PAPER

View Article Online
View Journal | View Issue

Cite this: *Soft Matter*, 2014, **10**, 990

X-ray tomography study of the random packing structure of ellipsoids

Chengjie Xia, Kuan Zhu, Yixin Cao, Haohua Sun, Binquan Kou and Yujie Wang*

Received 10th November 2013
Accepted 14th November 2013

DOI: 10.1039/c3sm52841c

www.rsc.org/softmatter

We present an X-ray tomography study for the random packing of ellipsoids. The local structure displays short-range correlations. In addition to the contact number Z, we introduce ρ_{shell}, the average contact radius of curvature for contacting neighbors, as an additional parameter to characterize the local orientational geometry. In general, the local free volume w is affected by both Z and ρ_{shell}. We believe that the particle asphericity induces a polydispersity effect to influence the packing properties. A model is introduced which explicitly maps the ellipsoid packing onto a polydispersed sphere one, and it reproduces most of the experimental observations.

I. Introduction

The study of random packing structures has attracted a lot of interest in recent years owing to its scientific importance and many engineering applications.[1–4] Most of the existing studies focus on random sphere packing.[5–8] However, for non-spherical particle packing, the additional rotational degree of freedom enriches the scope of packing problems[9] and increases the complexity for understanding the mechanical and rheological properties of various systems,[10] *e.g.* the stress transmission and distribution,[11] compaction process,[12–14] rheological properties,[15,16] glass transition phenomenon,[17,18] *etc.* The study of the microscopic geometry of non-spherical particle packing can help to understand all of the above properties.

On the other hand, the shape of a non-spherical constituent particle can be characterized through various shape parameters and they show respective effects on the packing structure.[19–22] Meanwhile, some universal properties of packed non-spherical particles have been observed, which has aroused wide interest among the community.[23] For instance, both spherocylinders and ellipsoids can have their random packing fractions vary non-monotonically as they deviate from spheres to very aspherical particles.[19,20,24] The maximum packing fractions attainable by varying the shape can be close to that of sphere crystal packing.[20,25] The non-monotonic effect has been explained by combining the contact number and the excluded volume effects.[19,20] To understand the macroscopic properties of packing, it is crucial to investigate its microscopic structures.[26,27] Nevertheless, the microscopic structures of non-spherical particle packing remain largely unexplored by experiments. It is therefore crucial to investigate how the microscopic structures are influenced by particle shapes, which in turn changes the macroscopic packing properties. The study of simple non-spherical packing, *e.g.* ellipsoid packing, can shed light on the understanding of random packing with particles of even more complex shapes.

In this study, we analyzed the detailed microscopic structure of random ellipsoid packing using the X-ray tomography technique to understand the non-spherical effects on the packing properties. We found that the spatial correlations in the packing were short-range, and the local fluctuations were induced mostly by an effective polydispersity effect. This effect is verified by a model, which explicitly maps particles with different orientations onto polydisperse spherical particles, and the corresponding polydisperse sphere packing can reproduce the experimentally observed fluctuations.

The paper is organized as follows. In Section II, we briefly describe our experimental setup and the image processing steps. In Section III, we define and calculate the distribution of various local parameters for the ellipsoid packing and their correlations. In Section IV, we propose an effective model which maps the asphericity effect onto a polydispersity effect, and compare the results with the experimental ones.

II. Experimental setup and image processing

The random ellipsoid packing structure was generated using M&M candies, following the original work by Donev *et al.*[20] The candies are oblate ellipsoids with average principal axes of $2a = 1.34$ cm and $2b = 0.69$ cm. About 4000 candies were poured into a cylindrical container with a 19 cm inner diameter. The container was tapped and shaken several times to compact the packing. The three-dimensional structures of three such packings were acquired using a Siemens® medical CT scanner with imaging resolution of about 0.6 mm. Standard image processing steps, including binarization and watershed

Department of Physics, Shanghai Jiao Tong University, 800 Dong Chuan Road, Shanghai 200240, China. E-mail: yujiewang@sjtu.edu.cn

segmentation,[28,29] were utilized to extract information including each particle's centroid and orientation $\vec{n}_i$ (Fig. 1). The particles had a size polydispersity of about 7%.

The average contact number $\langle Z \rangle$ was calculated to be about 9.8 using a generalized error-function fitting technique.[5,30] This method was also implemented to determine the volume of each particle, which yielded a global packing fraction of $\phi \approx 0.709$ for our packings. The values of $\langle Z \rangle$ and ϕ are consistent with other simulation and analytical works for ellipsoids with an aspect ratio close to our value: $\alpha \approx 0.51$.[20,23] The value of $\langle Z \rangle \approx 9.8$ further suggests that the iso-counting argument[31] for $\langle Z \rangle$, which is applicable to some other non-spherical particle packings including slender rod packings, also works for our ellipsoid packing.[31,32]

To minimize the boundary effect, further analysis was limited to particles which were a distance of $8b \approx 2.8$ cm away from the container boundary, leaving about 2200 particles in each packing structure.

III. Experimental results

A. Spatial correlations

To understand the structural correlations inside the packing structure, the pair correlation function (PCF) of the particle centroids was calculated and is shown in Fig. 2(a). The horizontal axis is scaled by $2b$. A broad first peak and a fast decay of the PCF were observed, which is in sharp contrast to that for spherical packings. The broad first peak can be easily explained by the non-spherical effect, since the centroid distance between two touching neighbors can vary from $2b$ to $2a \approx 1.93 \times 2b$, which roughly matches the width of the first peak. The rapid decay of the PCF beyond the first peak suggests a short-range position correlation.

In addition to the position correlation, a complex orientation correlation may arise in non-spherical particle packings, which can significantly affect the structural and mechanical properties.[4,11] The orientation pair correlation function is defined as:

$$S_2(r) = \langle P_2(\vec{n}_i \cdot \vec{n}_j) \delta(r - |\vec{r}_i - \vec{r}_j|) \rangle \quad (1)$$

where P_2 denotes the second order Legendre polynomial.[33] The result (Fig. 2(b)) shows that neighboring particles have a tendency to align with each other. The asymptotic value (≈ 0.079) at large r suggests a long-range nematic order. It turns out that this nematic order is along the gravity direction, $\vec{e}_z$, with the order parameter $S = \langle P_2(\vec{n}_i \cdot \vec{e}_z) \rangle \approx 0.226$.[33] Simulation work of the random deposition of ellipsoid particles suggests that the relative orientation of neighboring particles and the nematic order depend on the friction of the particles as well as the preparation method.[34,35] Our preparation method (pouring and shaking) imitates qualitatively a rapid quench followed by a slow annealing of the system. It is difficult to control the friction and preparation method in our experimental system.

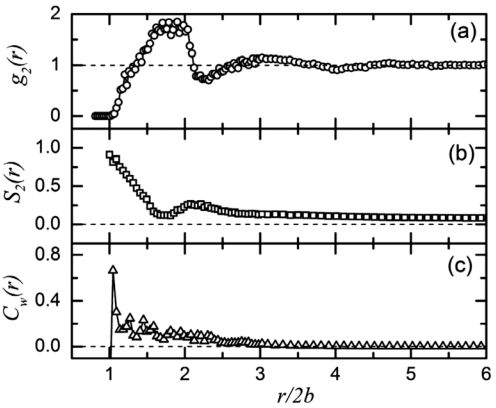

Fig. 2 (a) Pair correlation function. (b) Orientation pair correlation function. (c) Free volume pair correlation function.

The local free volume of a particle was obtained by navigation map tessellation[36,37] and is defined as the difference between the cell and the particle volume: $V_f = V_{cell} - V_0$ (different from $V_f = V_{cell} - V_{min}$ in the spherical case, where V_{min} is the minimum attainable volume[38]). The probability distribution function (PDF) of the normalized free volume, $w = V_f/V_0$, is shown in Fig. 3. Fig. 2(c) shows that w also has only a short-range spatial correlation.[39] The lack of long-range spatial correlations inside the packing suggests that the structural analysis can be limited to close neighbors.

B. Local contact geometry

Through navigation map tessellation, we could also define the number of nearest neighbors (N) for each particle. The distribution of N is shown in Fig. 4. For each neighbor, δ is defined as the nearest surface-to-surface distance between the central particle and itself, and the corresponding nearest pair of points on the respective surface are defined as the "facing" points. The distribution of δ is shown in Fig 5, which is in units of b. The

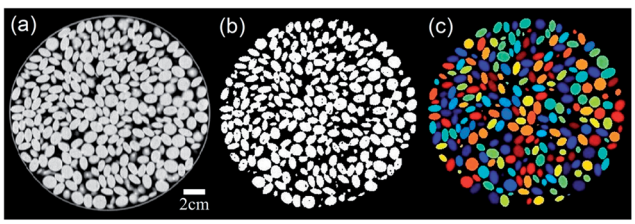

Fig. 1 Cross-sections of (a) a raw image, (b) a binary image, and (c) a segmented image.

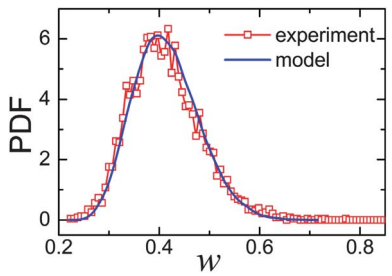

Fig. 3 PDF of the normalised free volume w: experimental data (squares) and model data (line).

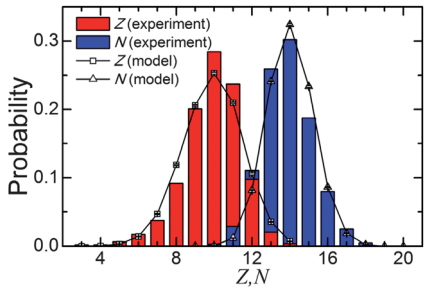

Fig. 4 Distribution of the number of nearest neighbors N: experimental data (blue bars) and simulation data (triangles). Distribution of contact number Z: experimental data (red bars) and simulation data (squares).

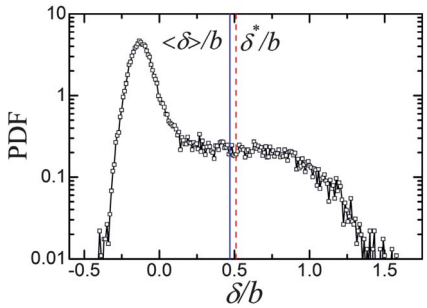

Fig. 5 PDF of δ. The solid line marks the average value of δ, and the dashed line marks δ^* as chosen by the model.

peak around zero is contributed to by contacting neighbors, while the non-contacting neighbors contribute to the flat distribution range and an exponential tail. Two particles are considered to be in contact if δ is within a threshold, determined by the aforementioned error-function fitting technique, and the corresponding "facing" points are defined as the contacting points. The Z contacting neighbors for each particle can be defined in this way and the Z distribution is shown in Fig. 4.

Other than N and Z, additional information is required to characterize the local structure around a ellipsoid particle. This is owing to the fact that both the contacting and non-contacting neighbors can have various orientations with respect to the central one, which is absent in sphere packings. To account for this, we defined a spherical coordinate system on each particle, where the origin coincides with the particle centroid and the polar axis is along its minor axis. To fix the relative position and orientation of two neighboring particles, the distance δ and the polar and azimuthal angles of the "facing" points of each particle on its respective coordinate systems have to be defined. When the local packing structure around a central particle is investigated in its own coordinate system, its azimuthal angle can be neglected owing to the rotational symmetry, which is not the case for its neighbors. Nevertheless, we ignored all the azimuthal angles of the neighbors by assuming that their contribution to the local packing properties was statistically averaged. It turns out that this assumption retains sufficient local packing information, while simplifying further analysis significantly. As shown in the two-dimensional schematic in Fig. 6(a), the contact geometry between two ellipsoids can therefore be simplified to a pair of contact angles $\{\theta_Z^{i,j}, \theta_Z^{j,i}\}$, where θ is the polar angle, and the notation with superscript (i, j) refers to the properties of the contact point on particle i which is in contact with particle j. The corresponding PDF is shown in Fig. 7. We subsequently define the contact radius of curvature $\rho_Z^{i,j}$, which is more relevant to the local structural properties, based on a Gaussian curvature (a good analytical approximation for the local curvature of our ellipsoids):

$$\rho_Z^{i,j} = \frac{a^2 \cos^2 \theta_Z^{i,j} + b^2 \sin^2 \theta_Z^{i,j}}{b}, \quad (2)$$

and its PDF $P(\rho_Z^{i,j})$ is shown in Fig. 8(a). The radius of curvature was made dimensionless by normalizing it with b. Similar calculations can be done for all neighbors by defining $\theta_N^{i,j}$ and $\rho_N^{i,j}$. Their PDFs are shown in Fig. 7 and 8(a), and are slightly different from those of $\theta_Z^{i,j}$ and $\rho_Z^{i,j}$. It is worth noting that their distributions are different from the PDFs assuming a uniform point distribution on the ellipsoid surface, as demonstrated by the solid curve in Fig. 7.

In the following, we use $\{\rho_Z^{i,j}, \rho_Z^{j,i}\}$ as the new measurement to characterize the relative orientation of contacting particles. There exists a rather weak correlation between $\rho_Z^{i,j}$ and $\rho_Z^{j,i}$ as shown in the inset of Fig. 7. This correlation corresponds to the fact that the sharp region of one particle has a small tendency to contact the sharp region of its neighbor, and so does the blunt region. This is consistent with the local alignments of particles, as evidenced by the orientational pair correlation function. However the correlation is rather weak, which enables us to neglect it and study the contact radii of curvature on the central particle and on contacting neighbors independently. To represent the different contact configurations with fewer degrees of freedom, we define the averages of $\{\rho_Z^{i,j}, \rho_Z^{j,i}\}$ as $\rho_{\text{center}} = \langle \rho_Z^{i,j} \rangle$ and $\rho_{\text{shell}} = \langle \rho_Z^{j,i} \rangle$, where the averages are taken over the contact points on the central particle (white dots, Fig. 6(a)) and on the contacting neighbors (black dots, Fig. 6(a)), respectively. These reduced variables are used subsequently to study their effects on properties like the contact number Z and the local free volume w.

C. Correlations of the local structural variables

The global distributions of ρ_{center} and ρ_{shell} are shown in Fig. 8(b), with variance values of $\sigma^2(\rho_{\text{center}}) \approx 0.012$ and $\sigma^2(\rho_{\text{shell}})$

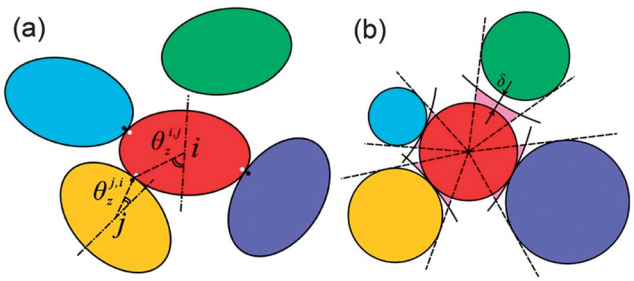

Fig. 6 Schematic diagrams of a local contact configuration and the polydispersed sphere model.

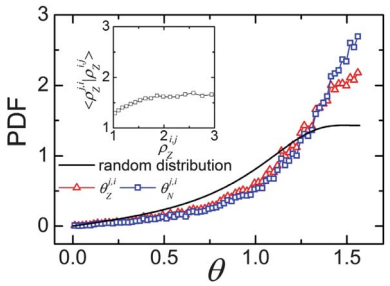

Fig. 7 The distribution of $\theta_Z^{j,i}$ and $\theta_N^{j,i}$. The solid line is the PDF assuming a uniform point distribution on the ellipsoid surface. Inset: the conditional average of $\rho_Z^{i,j}$ as a function of $\rho_Z^{j,i}$.

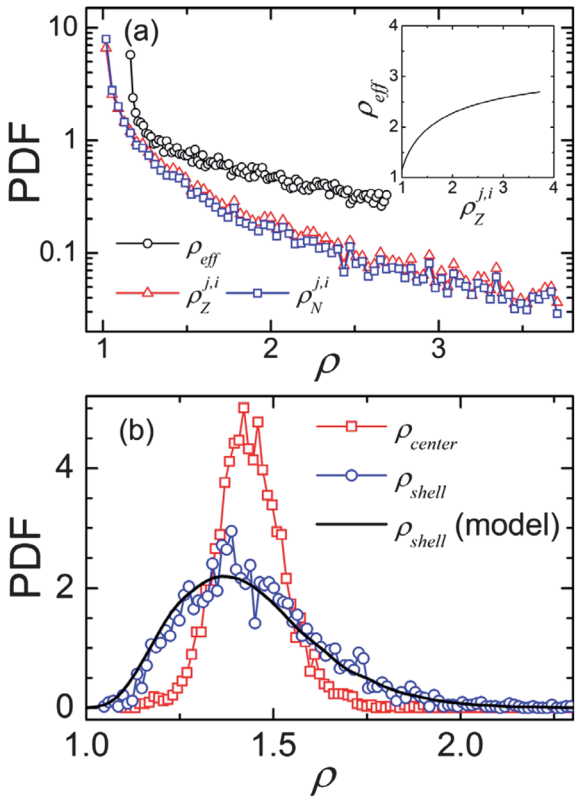

Fig. 8 (a) PDFs of $\rho_Z^{j,i}$ (triangles), $\rho_N^{j,i}$ (squares), and ρ_{eff} (circles). Inset: The relationship between ρ_{eff} and $\rho_Z^{j,i}$. (b) PDFs of ρ_{center} (squares) and ρ_{shell} (circles). The solid line is the PDF of ρ_{shell} from the model.

≈ 0.035. The substantial difference between their variance values suggests a different physical origin. Particularly, we believe that the value of $\sigma^2(\rho_{\text{shell}})$ originates from the fact that the contact radii of curvature for different contact neighbors with one central particle are totally uncorrelated. Meanwhile, the relatively small $\sigma^2(\rho_{\text{center}})$ value can be explained by the strong correlations among the contact points on the central particle due to steric effects. This steric effect can be demonstrated through the non-monotonic dependence of the conditional average of Z on ρ_{center}. As shown in Fig. 9(a), ρ_{center} deviates from its average value only when Z is small, while the dependence of N on ρ_{center} is comparatively weak.

In sharp contrast, ρ_{shell} turns out to be strongly correlated to N and Z. N and Z both decrease monotonically as ρ_{shell} increases (Fig. 9(a)), which is sensible since more particles are allowed to be placed around the central one if their sharp regions point towards the central particle. Interestingly, the ratio $p^* = \frac{\langle Z|\rho_{\text{shell}}\rangle}{\langle N|\rho_{\text{shell}}\rangle} \approx 0.71$, defined as the ratio of the conditional average of Z and N for a given range of ρ_{shell}, is approximately constant with varying ρ_{shell} (Fig. 9(b)).

Next we investigated how all of the relevant parameters determine w. We first demonstrated that the existence of the global nematic order hardly affects w, as the correlation coefficient between them equals a rather small number of 0.082. It is reasonable that ρ_{shell} should influence w, which is clearly different from that in sphere packings where the free volume is determined by the average contact number Z alone.[6] We classified all particles based on their ρ_{shell} and Z values, and plotted the conditional average of the free volume $\langle w\rangle$ *versus* ρ_{shell} for each Z value to display more explicitly their respective dependency on w. As shown in Fig. 10(a), for each fixed Z value, $\langle w\rangle$ decreases as ρ_{shell} increases, which can be understood by the fact that the blunt region on a neighboring ellipsoid blocks more free volume than its sharp region. Similarly, $\langle w\rangle$ decreases

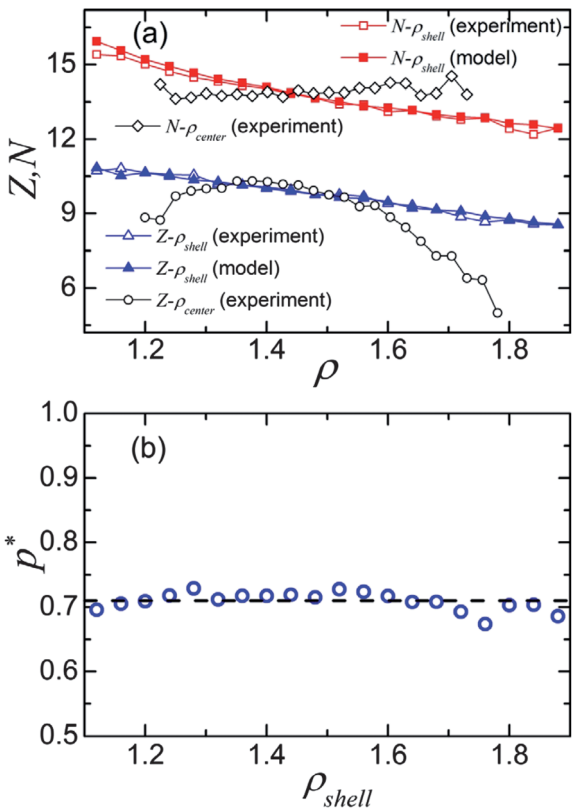

Fig. 9 (a) The conditional average of the neighbor number N as a function of ρ_{center} (diamonds), ρ_{shell} (open squares), and ρ_{shell} (model data, solid squares). The conditional average of the contact number Z as a function of ρ_{center} (circles), ρ_{shell} (open triangles), and ρ_{shell} (model data, solid triangles). (b) The ratio between the conditional average of Z and N: $p^* = \frac{\langle Z|\rho_{\text{shell}}\rangle}{\langle N|\rho_{\text{shell}}\rangle}$, as a function of ρ_{shell}.

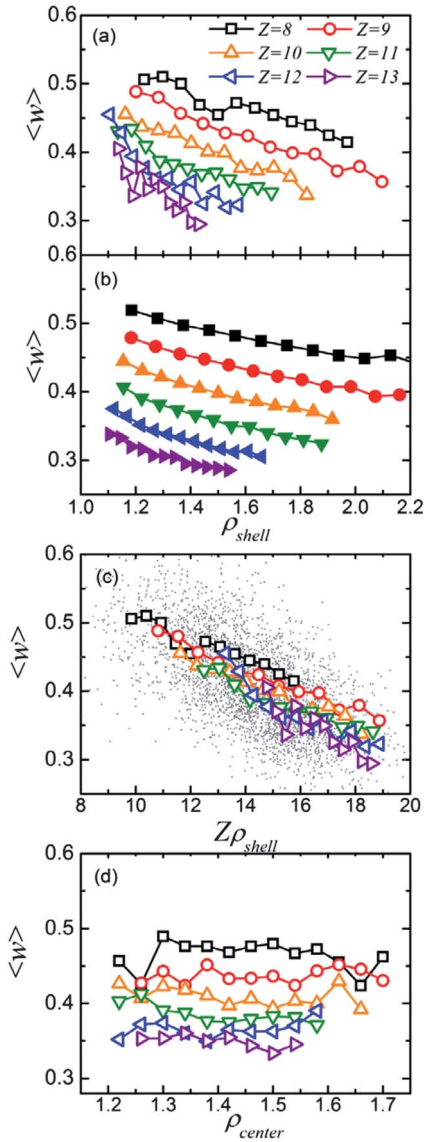

Fig. 10 Experimental data (a) and model data (b) for the conditional average of the free volume w *versus* ρ_{shell} for contact number Z. (c) Conditional average of the free volume $\langle w\rangle$ *versus* $Z\rho_{\mathrm{shell}}$. The scatter points are the unaveraged experimental data points. (d) Conditional average of the free volume w *versus* ρ_{center} for contact number Z.

as Z increases for a fixed ρ_{shell} value. All curves collapse onto a single curve if $\langle w\rangle$ is plotted against $Z\rho_{\mathrm{shell}}$, as shown in Fig. 10(c). A similar analysis was done for the relationship between w and ρ_{center}, and $\langle w\rangle$ was almost constant when varying ρ_{center} for a fixed Z value (Fig. 10(d)). This shows that for a fixed Z value, ρ_{center} introduces a very small fluctuation in the free volume w.

IV. Model

The dependence of w on ρ_{shell} suggests that particle asphericity can induce an "effective" polydispersity effect to influence the packing properties. In this section, we introduce a simple polydisperse sphere particle packing model to further clarify this concept and use the model to account for the observed local packing properties and fluctuations. The model is illustrated in Fig. 6. To account for the local packing environment, the central ellipsoid is approximated simply by a sphere with a fixed radius $r_c = (3V_0/4\pi)^{\frac{1}{3}} \approx 1.55b$. This is owing to its weak impact on the local packing properties due to the strong steric correlation at our particular ellipsoid aspect ratio. The neighboring ellipsoids, on the other hand, are mapped onto spheres with different ρ_{eff} values as follows. First the radii of curvature ρ of all the neighbors are assumed to follow the same PDF of $P(\rho_Y^{j,i})$ despite the small difference between the PDFs of $\rho_Z^{j,i}$ and $\rho_N^{j,i}$. Then we determined a sphere of radius ρ_{eff}, which can subtend the same solid angle on the aforementioned central sphere as that of a contacting ellipsoid whose contact radius of curvature is ρ. There exists a one-to-one correspondence between ρ_{eff} and ρ, as shown in the inset of Fig. 8(a). By mapping the ellipsoids onto polydisperse sphere particles, we end up with a polydisperse sphere packing problem with the PDF of ρ_{eff} as shown in Fig. 8(a).

With the above approximations and the mapping of our packing onto a polydisperse sphere packing, the "Granocentric" model, which was originally introduced to study polydisperse packings, can be implemented to calculate various local packing properties.[7,40] The "Granocentric" model approximates the formation of the local geometry as a local stochastic process by selecting neighboring particles of different sizes randomly from the distribution and determining whether the neighbor contacts with the central particle through a Bernoulli trial with a fixed probability. There are three control parameters (p^*, δ^* and Ω^*) in the model. The parameter p^* is the probability that one neighbor contacts with the central particle, and we used $p^* = 0.71$, according to the experimental value (Fig. 9(b)). The parameter δ^* is the surface-to-surface distance of non-contacting neighbors with the central particle, while the parameter Ω^* is the upper limit of the total solid angle subtended on the central particle by all neighbors. Experimentally, there is a broad distribution of δ (Fig. 5) and it is not independent of Z and ρ_{shell}. To show the interdependence of δ on Z and ρ_{shell}, we defined Δ as the average δ between each central particle and all its non-contacting neighbors. Basically Δ varies with Z and ρ_{shell}, so we classified particles based on Z and ρ_{shell}, and plotted $\langle\Delta\rangle$ (the conditional average of Δ) as a function of ρ_{shell} for different Z values, as shown in Fig. 11(a). Surprisingly, all the curves for different Z values also collapsed onto a single curve when plotted against $Z\rho_{\mathrm{shell}}$, showing a similar behavior to w (Fig. 11(b)). However, similar to the spherical case, we simplified the model by using a single value of δ, which can reproduce most of the experimentally observed fluctuations. This suggests that the fluctuations are mainly determined by the polydispersity effect induced by asphericity rather than the positional disorder characterized by δ.[41]

The local configurations could then be generated following the same procedure as the original "Granocentric" model.[7,40] The N, Z and w values could be obtained for each simulated configuration. Simulated ρ_{shell} is defined as the average radius ρ of all contacting neighbors. We tuned δ^* and Ω^* so that $\langle N\rangle$, $\langle Z\rangle$

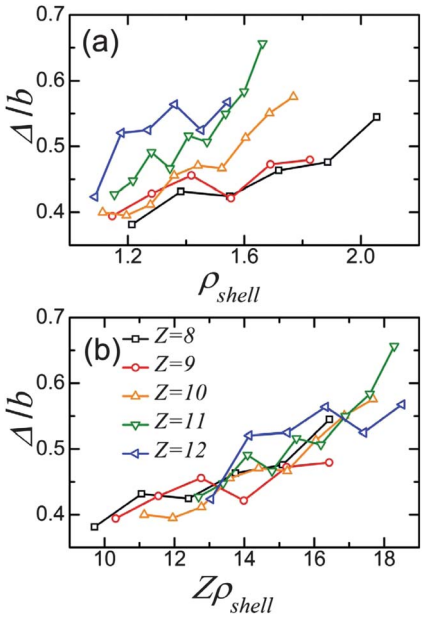

Fig. 11 Conditional average of Δ for different contact numbers Z *versus* (a) ρ_{shell} and (b) $Z\rho_{\mathrm{shell}}$.

and $\langle w \rangle$ matched their experimental counterparts simultaneously. The optimized δ^* value was $0.51b$ and the optimized Ω^* value was 3.87π. In the experiments, the average δ value of the central particles and their non-contacting neighbors was $0.47b$. The scatter plot of Ω_{tot} (the total solid angle subtended on the central particle by all the neighbors) *versus* ρ_{shell} for experimental data suggests that the assumption that Ω^* is independent of ρ_{shell} is appropriate, while $\Omega^* = 3.87\pi$ seems slightly larger than the experimental values (Fig. 12). This may be due to the fact that the surface area of the central sphere in the model is smaller than the ellipsoid of the same volume.

Ten thousand such simulated configurations were generated to be compared with the experimental results. First of all, the distribution of simulated ρ_{shell} agrees nicely with its experimental counterpart (Fig. 8(b)), justifying the assumption that the radii of curvature of contacting neighbors are uncorrelated. The correlations between N, Z and ρ_{shell} are perfectly reproduced by the model as shown in Fig. 9(a), justifying the polydispersity picture. The distributions of N, Z and w are also successfully obtained (Fig. 3 and 4). In general, the free volume dependence on Z and ρ_{shell} matches well with the experimental data (Fig. 10(b)), which further justifies the validity of the polydispersity picture.

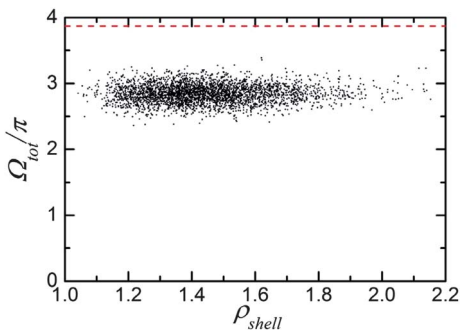

Fig. 12 A scatter plot showing $\frac{\Omega_{\mathrm{tot}}}{\pi}$ *versus* ρ_{shell} for experimental data. The dashed line marks $\Omega^* = 3.87\pi$ as chosen by the model.

V. Conclusions

In conclusion, we have carried out an experimental study on the packing structures of ellipsoids using the X-ray tomography technique. We found that the packing lacked long-range spatial correlations. The local contact geometry was characterized by the contact number Z and the averaged contact radius of curvature ρ_{shell} to determine the local free volume w. The parameter ρ_{shell} was introduced to approximate the effective polydispersity effect induced by the particle orientations. A simple polydisperse sphere model adopting this approximation reproduced most of the experimental results for real ellipsoid packing structures. The applicable scope of the above assumption for non-spherical packing structures with various aspect ratios and different shapes awaits further studies.

Acknowledgements

The work is supported by the Chinese National Science Foundation no. 11175121, and the National Basic Research Program of China (973 Program; 2010CB834301).

References

1 T. Aste and D. Weaire, *The pursuit of perfect packing*, 2008.
2 S. F. Edwards and R. B. S. Oakeshott, *Phys. A*, 1989, **157**, 1080–1090.
3 A. J. Liu and S. R. Nagel, *Nature*, 1998, **396**, 21–22.
4 S. Torquato and F. H. Stillinger, *Rev. Mod. Phys.*, 2010, **82**, 2633–2672.
5 T. Aste, M. Saadatfar and T. Senden, *Phys. Rev. E: Stat., Nonlinear, Soft Matter Phys.*, 2005, **71**, 061302.
6 C. Song, P. Wang and H. A. Makse, *Nature*, 2008, **453**, 629–632.
7 M. Clusel, E. I. Corwin, A. O. N. Siemens and J. Brujić, *Nature*, 2009, **460**, 611–615.
8 M. Danisch, Y. Jin and H. A. Makse, *Phys. Rev. E: Stat., Nonlinear, Soft Matter Phys.*, 2010, **81**, 051303.
9 S. C. Glotzer and M. J. Solomon, *Nat. Mater.*, 2007, **6**, 557–562.
10 T. Börzsönyi and R. Stannarius, *Soft Matter*, 2013, **9**, 7401.
11 R. Hidalgo, I. Zuriguel, D. Maza and I. Pagonabarraga, *Phys. Rev. Lett.*, 2009, **103**, 118001.
12 F. X. Villarruel, B. E. Lauderdale, D. M. Mueth and H. M. Jaeger, *Phys. Rev. E: Stat. Phys., Plasmas, Fluids, Relat. Interdiscip. Top.*, 2000, **61**, 6914–6921.
13 G. Lumay and N. Vandewalle, *Phys. Rev. E: Stat., Nonlinear, Soft Matter Phys.*, 2004, **70**, 051314.
14 Y. Fu, Y. Xi, Y. Cao and Y. Wang, *Phys. Rev. E: Stat., Nonlinear, Soft Matter Phys.*, 2012, **85**, 051311.

15 T. Börzsönyi, B. Szabó, G. Törös, S. Wegner, J. Török, E. Somfai, T. Bien and R. Stannarius, *Phys. Rev. Lett.*, 2012, **108**, 228302.
16 S. Farhadi, R. P. Behringer and A. Z. Zhu, *AIP Conf. Proc.*, 2013, **1542**, 879–882.
17 Z. Zheng, F. Wang and Y. Han, *Phys. Rev. Lett.*, 2011, **107**, 065702.
18 C. K. Mishra, A. Rangarajan and R. Ganapathy, *Phys. Rev. Lett.*, 2013, **110**, 188301.
19 S. Williams and A. Philipse, *Phys. Rev. E: Stat., Nonlinear, Soft Matter Phys.*, 2003, **67**, 051301.
20 A. Donev, I. Cisse, D. Sachs, E. A. Variano, F. H. Stillinger, R. Connelly, S. Torquato and P. M. Chaikin, *Science*, 2004, **303**, 990–993.
21 A. Jaoshvili, A. Esakia, M. Porrati and P. M. Chaikin, *Phys. Rev. Lett.*, 2010, **104**, 185501.
22 N. Gravish, S. V. Franklin, D. L. Hu and D. I. Goldman, *Phys. Rev. Lett.*, 2012, **108**, 208001.
23 A. Baule, R. Mari, L. Bo, L. Portal and H. A. Makse, *Nat. Commun.*, 2013, **3194**(4), 2194.
24 S. Sacanna, L. Rossi, A. Wouterse and A. P. Philipse, *J. Phys.: Condens. Matter*, 2007, **19**, 376108.
25 W. Man, A. Donev, F. Stillinger, M. Sullivan, W. Russel, D. Heeger, S. Inati, S. Torquato and P. M. Chaikin, *Phys. Rev. Lett.*, 2005, **94**, 198001.
26 A. Donev, R. Connelly, F. Stillinger and S. Torquato, *Phys. Rev. E: Stat., Nonlinear, Soft Matter Phys.*, 2007, **75**, 051304.
27 C. F. Schreck, M. Mailman, B. Chakraborty and C. S. O'Hern, *Phys. Rev. E: Stat., Nonlinear, Soft Matter Phys.*, 2012, **85**, 061305.
28 Y. Cao, B. Chakraborty, G. C. Barker, A. Mehta and Y. Wang, *Europhys. Lett.*, 2013, **102**, 24004.
29 A. Gillman, K. Matouš and S. Atkinson, *Phys. Rev. E: Stat., Nonlinear, Soft Matter Phys.*, 2013, **87**, 022208.
30 F. M. Schaller, M. Neudecker, M. Saadatfar, G. Delaney, K. Mecke, G. E. Schröder-Turk and M. Schröter, *AIP Conf. Proc.*, 2013, **1542**, 377–380.
31 J. Blouwolff and S. Fraden, *Europhys. Lett.*, 2006, **76**, 1095–1101.
32 A. Wouterse, S. Luding and A. P. Philipse, *Granular Matter*, 2009, **11**, 169–177.
33 B. J. Buchalter and R. M. Bradley, *Europhys. Lett.*, 1994, **26**, 159–164.
34 B. Buchalter and R. Bradley, *Phys. Rev. A: At., Mol., Opt. Phys.*, 1992, **46**, 3046–3056.
35 G. W. Delaney, J. E. Hilton and P. W. Cleary, *Phys. Rev. E: Stat., Nonlinear, Soft Matter Phys.*, 2011, **83**, 051305.
36 E. N. Gilbert, *Ann. Math. Stat.*, 1962, **33**, 958.
37 F. M. Schaller, S. C. Kapfer, M. E. Evans, M. J. F. Hoffmann, T. Aste, M. Saadatfar, K. Mecke, G. Delaney and G. E. Schröder-Turk, *Philos. Mag.*, 2013, **93**, 3993.
38 T. Aste and T. Di Matteo, *Phys. Rev. E: Stat., Nonlinear, Soft Matter Phys.*, 2008, **77**, 021309.
39 S. Zhao, S. Sidle, H. L. Swinney and M. Schröter, *Europhys. Lett.*, 2012, **97**, 34004.
40 K. A. Newhall and J. Ivane, *Soft Matter*, 2011, **7**, 11518–11525.
41 K. A. Newhall, L. L. Pontani, I. Jorjadze, S. Hilgenfeldt and J. Brujic, *Phys. Rev. Lett.*, 2012, **108**, 268001.